Hybrid ECM and LSTM Approach for State-of-Health Estimation of Lithium-ion Batteries

Chatcharan Yomjinda
Advanced Mobility and Propulsion Research Laboratory,
Faculty of Engineering,
Thai-Nichi Institute of Technology
Bangkok, THAILAND
*Author: 2461110021@tni.ac.th

Mahunnop Fakkao
Advanced Mobility and Propulsion Research Laboratory,
Faculty of Engineering,
Thai-Nichi Institute of Technology l
Bangkok, THAILAND
*Corresponding author: mahunnop@tni.ac.th

Abstract— Lithium-ion batteries (LiBs) have become the leading energy storage technology for electric vehicle applications due to their high energy density and compact size. To improve operational efficiency and ensure safe operation, battery management systems (BMSs) monitor battery health. However, accurately diagnosing and predicting the State of Health (SOH) remains a significant challenge. Although purely data-driven methods have shown high predictive accuracy, they often lack physical interpretability and fail to explain underlying electrochemical degradation mechanisms. This study introduces a long short-term memory (LSTM) framework integrated with electrochemical impedance spectroscopy (EIS) data to achieve both high prediction accuracy and deeper mechanistic understanding. Nyquist plots obtained from EIS were fitted using an equivalent circuit model (ECM) to extract physical parameters, including ohmic resistance, electrolyte resistance, charge-transfer resistance, and the Warburg coefficient. These features, along with capacity, were used as inputs for the LSTM model. The model was trained and validated using SOH labels derived from capacity measurements of four commercial pouch cell NMC lithium-ion batteries with a nominal reversible capacity of 2 Ah. Validation was conducted on an additional cell over 100 aggressive continuous charge–discharge cycles at 2.5 C and 100% Depth of Discharge. Analytical results using Pearson correlation and feature-importance algorithms identified the Warburg impedance (R_w) as the key parameter for early capacity fade, reflecting obstructed solid-state diffusion due to severe structural strain. Conversely, charge-transfer resistance (R_{ct}) showed a positive correlation indicative of a temporary cell activation and deep electrolyte wetting phase. The proposed EIS-driven framework effectively bridges the gap between predictive accuracy and physical interpretability, offering a practical and reliable approach for next-generation BMS applications.

Keywords—Lithium-ion battery, State-of-Health Estimation, Electrochemical Impedance Spectroscopy, Equivalent Circuit Model, Long Short-Term Memory

I. INTRODUCTION

The electrification of the transportation sector is a critical strategy for mitigating global carbon emissions, with the Electric Vehicle (EV) emerging as a primary solution. The core component of an EV powertrain system is the lithium-ion battery (LIB), whose performance, longevity, and safety are regulated by a Battery Management System (BMS). A crucial function of BMS is to estimate the State-of-Health (SOH), a metric that represents the battery's remaining useful capacity relative to its initial state. For automotive applications, LIBs are generally considered to have reached the end of life (EOL) when SOH degrades to 70-80% [1].

Battery degradation is a complex phenomenon driven by various electrochemical mechanisms, including low-temperature operation, high C-rate cycling, electrolyte decomposition, and mechanical stress. In Nickel Manganese Cobalt (NMC) LIBs, the capacity fade is primarily attributed to the growth of solid electrolyte interfaces (SEIs), lithium plating, electrode decomposition, and active material fracturing. Collectively, these mechanisms lead to an increase in internal resistance and a corresponding fade in capacity]2[.

Currently, there are three main approaches to diagnosing battery health and predicting SOH. First, state-of-the-art spectroscopic techniques, such as X-ray absorption spectroscopy (XAS), utilize synchrotron radiation to probe local atomic structures and element-specific oxidation state [3, 5]. Furthermore, imaging techniques such as 2D-XAS Imaging and Computed Tomography XAS enable visualization of the temporal and spatial distribution and morphological changes within electrode materials [7]. While these methods provide exceptional localized diagnostic precision for phenomena such as particle cracking and heterogeneous state-of-charge distributions, they require large-scale facilities and complex offline analysis. Consequently, they remain impractical for real-time onboard implementation in commercial BMS applications.

Secondly, model-based methods typically use electrochemical impedance spectroscopy (EIS) to estimate the parameters of equivalent circuit models (ECMs). These models extract parameters such as charge-transfer resistance (R_{ct}) and double-layer capacitance (C_{dl}) to reflect internal physicochemical states [8, 9]. While ECMs offer excellent physical interpretability, they struggle to accurately replicate the highly non-linear dynamic behavior of LIBs under aggressive load profiles without incurring high computational cost [10-12]. Conversely, simplified models, such as the Single Particle Model [13], reduce the computational burden but often sacrifice predictive accuracy.

Finally, data-driven methods have rapidly become the leading approach to battery health estimation, propelled by advances in artificial intelligence and computational power. Deep learning models, particularly Recurrent Neural Networks (RNNs) and Long Short-Term Memory (LSTM) networks, are highly effective at capturing complex, nonlinear electrochemical behaviors without requiring explicitly defined physical parameters. However, these models suffer from the black box problem. By translating inputs into outputs via hidden layers that lack physical meaning, purely data-driven models often fail to reveal the root causes of degradation, raising reliability concerns for safety-critical BMS applications [14-16]

To address the trade-off between physical interpretability and predictive accuracy, this study proposes a Hybrid ECM-integrated LSTM framework. This approach utilizes an EIS-based ECM to extract physics-informed features, *i.e.*, changes in internal resistance that correlate with physical degradation mechanisms. These extracted features serve as inputs for the LSTM network, which is inherently designed to capture long-term dependencies in time-series data [17-19]. Unlike previous hybrid studies [20-22] that prioritized computational efficiency, this framework integrates the mechanistic diagnostic capabilities of ECMs with the non-linear predictive power of deep learning, offering a robust and interpretable solution for real-time SOH estimation.

II. METHODOLOGY

A. Experimental setup

This study used five commercial pouch-cell-type NMC-based LIBs, each with a measured nominal capacity of approximately 2 Ah. To accelerate degradation mechanisms, the cells were subjected to 100 aggressive charge-discharge cycles using a potentiostat/galvanostat (BioLogic VSP-3e) with a current booster (BioLogic VMP3B-5). The cycling protocol applied a continuous current of 5 A, corresponding to a 2.5 C-rate, over the voltage range of 3.0-4.2V. Specifically, the discharge phase utilized a Constant Current-Constant Voltage (CC-CV) profile, discharging the cell to 3.0 V and holding at this voltage until the current tapered below 1 mA, ensuring a strict 100% Depth of Discharge (DOD). At the end of charging and discharging processes, EIS was employed as detailed in Table 1. The continuous capacity fade observed across the 100 cycles served as the primary indicator of degradation, which was subsequently quantified to determine the SOH of the cells as expressed in (1)

$$SOH(\%) = \frac{C_r}{C_0} \times 100 \tag{1}$$

where C_r is the remaining capacity, and C_0 is the initial capacity.

TABLE I. EXPERIMENTAL CONDITION SETTINGS

State	Experimental condition setting		
	Procedure	***limits***	***T (℃)***
1	Rest time	5 min	25℃
2	EIS 10 mV from 10kHz to 10mHz	15 min	
3	Rest time	5 min	
4	CC-CV charge(I= 5 A, Cut-off voltage =4.2V, I_limit=1 mA)	3V to 4.2V	
5	Rest time	30 min	
6	EIS 10 mV from 10kHz to 10mHz	15 min	
7	Rest time	30 min	
8	CC-CV discharge (I=5 A,Cut-off Voltage=3.0 V, I_limit = 1 mA)	4.2V to 3V	

B. Equivalent Circuit model

To extract the internal resistance value, the Nyquist plots obtained from EIS measurement were fitted to an equivalent circuit model (ECM) as shown in Fig. 1. The curve fitting process extracted physical parameters, including ohmic resistance (R_O), solid electrolyte interphase resistance (R_s), charge-transfer resistance (R_{ct}) and Warburg resistance for Li-ion diffusion (R_W). The impedance of the battery, $Z_{LIB}\,(\omega)$, is represented as a function of frequency (ω) by the equation (2)

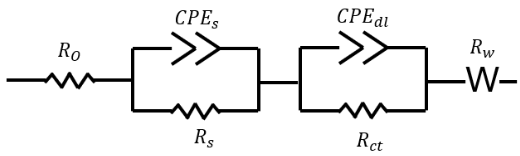

Fig. 1. The equivalent circuit model in this study

$$Z_{LIB}\,(\omega) = R_O + \frac{R_s}{1 + R_s(j\omega)^{\alpha s}Q_s} + \frac{R_{ct}}{1 + R_{ct}(j\omega)^{\alpha dl}Q_{dl}} + \frac{R_w coth\sqrt{j\omega\sigma}}{\sqrt{j\omega\sigma}} \tag{2}$$

where Q_s, Q_{dl} represents the pseudo-capacitance of electrolyte interphase and electrode surface, respectively, α is the degree of non-ideality in the electrical response, and σ is the Warburg coefficient.

C. ECM Validation

To evaluate the predictive performance of ECM curve fitting, the coefficient of determination (R^2) and the root mean square error (RMSE) were calculated as expressed in (3) and (4), respectively.

$$R^2 = 1 - \frac{\sum_{i=1}^{n}(y_i - \hat{y_i})^2}{\sum_{i=1}^{n}(y_i - \bar{y})^2} \tag{3}$$

$$RMSE = \sqrt{\frac{1}{n}\sum_{i=1}^{n}(y_i - \hat{y_i})^2} \tag{4}$$

where n is the number of parameters, y_i are the actual values, $\hat{y_i}$ are the predicted values, and $\bar{y}$ is the mean of the actual values.

Furthermore, a Pearson correlation analysis was employed to quantify the relationship between extracted resistance parameters and SOH over 100 cycles. The Pearson correlation coefficient (r) is $r$calculated as (5).

$$r = \frac{\sum(x_i - \bar{x})(y_i - \bar{y})}{\sqrt{\sum(x_i - \bar{x})^2 \sum(y_i - \bar{y})^2}} \tag{5}$$

where x_i is fitting resistance, y_i is SOH, $\bar{x}$ is the average of fitting resistance, and $\bar{y}$ is the average of SOH. To determine the confidence interval (CI) for r, Fisher's transformation was applied to address the asymmetry of the probability distribution as r is bounded between -1 and 1. The transformation (F) and standard error (SE) are defined as (6), and (7), respectively.

$$F = \frac{1}{2}\ln(\frac{1+r}{1-r}) \quad (6)$$

$$SE = \frac{1}{\sqrt{n-3}} \quad (7)$$

The 95% CI is then calculated using the Z-score for the 95% confidence interval, as given in (8).

$$CI = F \pm Z \times SE \quad (8)$$

D. *Long Short-Term Memory (LSTM) Model Design*

For the LSTM model development, the key resistance parameters (R_O, R_s, R_{ct},R_w) extracted from the ECM were selected as input features. Based on the hypothesis that these resistance parameters are inversely related to electrochemical characteristics, battery capacity (C) was incorporated as an additional input feature to maintain balance in the LSTM model, with SOH designated as the target output. The dataset was divided into two subsets: data from four cells (cells 1-4) were used for training, and data from the fifth cell (Cell 5) were reserved for testing.

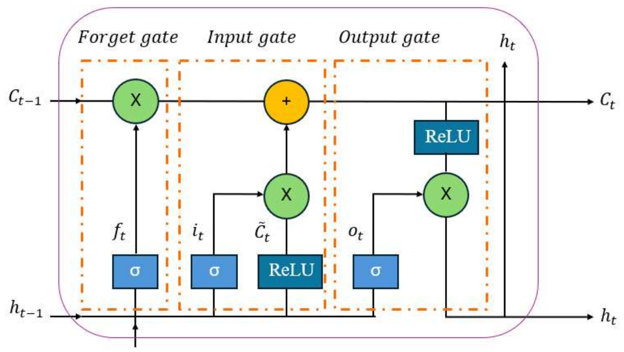

Fig. 2. LSTM architecture

The LSTM architecture processes data through three distinct gates, *i.e.*, the forget gate (f_t), the input gate (i_t), and the output gate (o_t) as shown in Fig. 2. The gate operations are defined by (9)-(11).

$$f_t = \sigma(W_f * [h_{t-1}, x_t] + b_f \quad (9)$$

$$i_t = \sigma(W_i * [h_{t-1}, x_t] + b_i \quad (10)$$

$$o_t = \sigma(W_o * [h_{t-1}, x_t] + b_o \quad (11)$$

where σ represents the sigmoid activation function, which outputs values between 0 and 1. W_f, W_i, and W_o denote the weight matrices for the forget, input, and output gates, respectively, while b_f, b_i, and $b_o$are the corresponding bias vectors for each gate. The term $[h_{t-1}, x_t]$ represents the concatenation of the previous hidden state and the current input feature vector.

The forget gate determines which information from the previous cell state to discard, the input gate decides which new information to store, and the output gate determines the next hidden state based on the updated cell state. To avoid the vanishing gradient problem, the model employed a Rectified Linear Unit (ReLU) activation function for the cell state updates as expressed in (12)-(14).

$$\tilde{C}_t = ReLU(W_c * [h_{t-1}, x_t] + b_c) \quad (12)$$

$$C_t = f_t * C_{t-1} + i_t * \tilde{C}_t \quad (13)$$

$$h_t = o_t * ReLU(C_t) \quad (14)$$

where $\tilde{C}_t$ is the candidate cell state containing new information, $C_t$and C_{t-1} are the current and previously cell states, h_t is the hidden cell state of the current input.

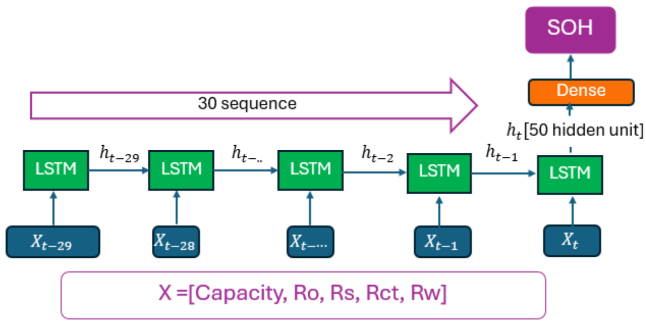

Fig. 3. Many-to-one structure of LSTM

The model was designed with a many-to-one architecture, as illustrated in Fig 3. It consists of a single LSTM hidden layer containing 50 hidden units. To prevent overfitting during training, a dropout layer with a rate of 0.5 (50%) is applied immediately after the LSTM layer. The signal is then passed to a dense layer with a single output node to predict battery capacity, which is subsequently converted to SOH. The model is optimized using the Adaptive Moment Estimation (Adam) optimizer with a learning rate of 0.0005, processing the input time-series data through a time-step window of 30 cycles (sequence length = 30).

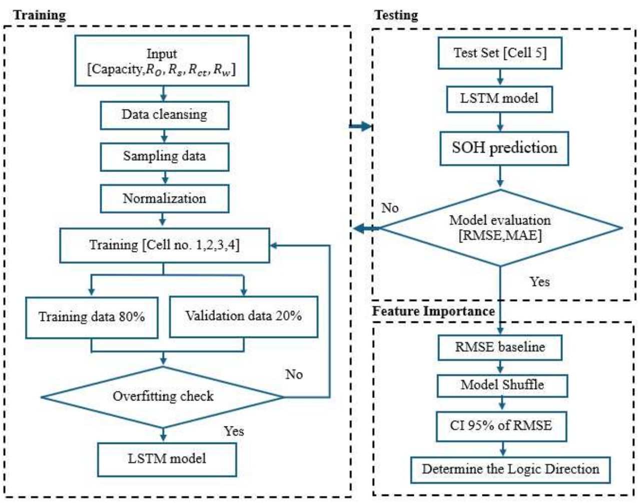

Fig. 4. Overall framework of LSTM modeling and feature importance.

E. Model Evaluation and Feature Importance

The predictive performance of the LSTM model was quantitatively evaluated using RMSE, as (4), and mean absolute error (MAE) as expressed in (15)

$$MAE = \frac{1}{n}\sum_{i=1}^{n}|y_i - \hat{y_i}| \qquad (15)$$

To interpret the model's decision-making process, a feature-importance algorithm was developed to identify the most impactful resistance feature for Cell 5. The algorithm consists of the following steps:

1. Calculate RMSE baseline: the RMSE derived from the prediction validation is established as the reference baseline.
2. Model Shuffle: the sequence of each resistance parameter is randomly shuffled one at a time with 50 iterations per parameter, and RMSE is recalculated for each instance.
3. Confidence interval of RMSE: The recalculated 50 RMSE values for each parameter are used to calculate the 95% CI (16).

$$CI = \overline{RMSE} \pm Z \times \frac{SD}{\sqrt{n}} \qquad (16)$$

where $\overline{RMSE}$ is the average of RMSE, Z is the Z-score for CI 95%, *i.e.*, a constant value of 1.96 in this case, SD is the standard deviation of RMSE, and n is the number of random shuffles (n = 50).

4. Determine the Logic Direction: The model is evaluated by slightly increasing a feature's value to observe whether the predicted SOH responds positively or negatively.

The overall framework of the proposed SOH estimation system is illustrated in Fig. 4.

III. Results and Discussion

A. Pearson Correlation Analysis

The Pearson correlation method was utilized to establish the relationship between the extracted ECM's resistance parameters and SOH over 100 cycles, evaluated at a 95% CI, 95% as shown in Fig. 5. The results, represented by a combination bar chart and error bars, indicate distinct positive (red bar) and negative (green bar) correlations across two axes. As anticipated, the battery capacity exhibited a positive correlation with SOH, consistent with capacity decreasing with SOH per cycle. Among the internal resistance parameters, the charge-transfer resistance (R_{ct}) uniquely demonstrated a positive correlation. Conversely, the Warburg diffusion resistance (R_w), solid electrolyte interphase resistance (R_s), and ohmic resistance (R_O) all exhibited negative correlations.

When evaluating parameter importance using the average Pearson correlation coefficient (r), the strongest negative correlation interval was identified as [-0.668 ± 0.119]. This was followed by R_s at [-0.454 ± 0.1725] and R_O at [-0.366 ± 0.189]. The positive correlation for R_{ct} was measured at [0.379 ± 0.187].

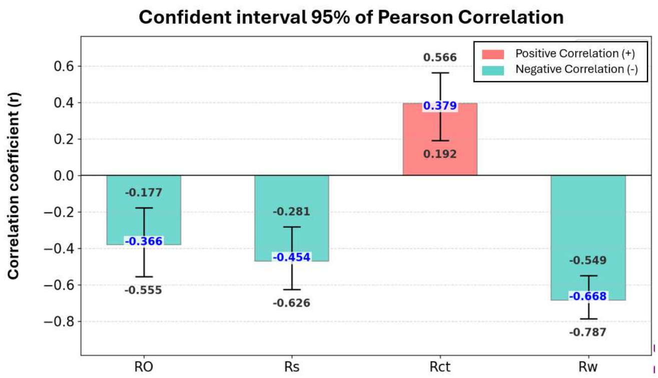

Fig. 5. Pearson correlation of each resistance obtained from ECM at 95% Confidence Interval.

B. LSTM Model Prediction Performance

The predictive performance of the LSTM was assessed by comparing predicted SOH with actual SOH across the tested cycles. The red dashed line showed that the predicted values closely followed the actual SOH trend (blue scatter dot), effectively capturing the gradual degradation as the cycle count increased, as illustrated in Fig. 6. The overall prediction accuracy of the model was quantitatively validated, achieving an RMSE of 1.151% and an MAE of 0.875%. This established RMSE was subsequently used as the baseline reference for the feature-importance processing algorithm.

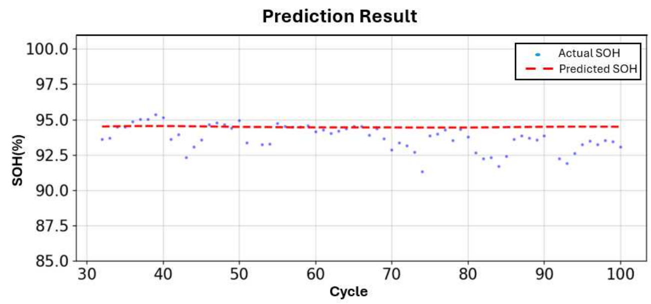

Fig. 6. LSTM predicted SOH vs. actual SOH.

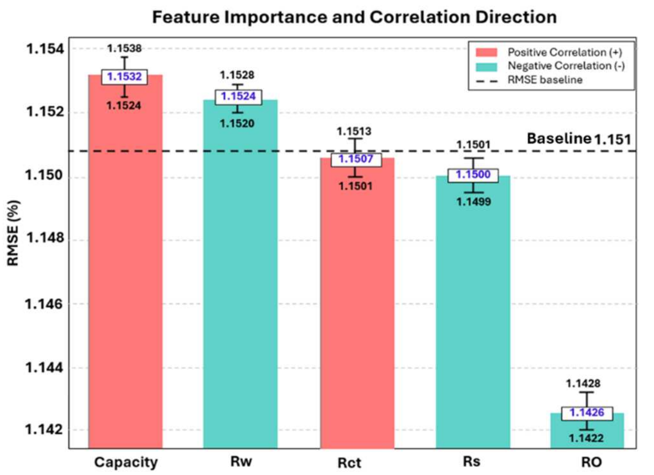

Fig. 7. Important resistance parameter and its correlation with the SOH prediction of cell 5 at 95% confidence interval.

C. Feature Importance of Impedance Parameters

A feature importance algorithm was implemented to identify the specific impact of each resistance parameter on the model's predictive accuracy, using the 95% RMSE CI. Fig. 7 shows the importance and correlation of each resistance parameter on SOH prediction. The red and green bars represent the positive and negative correlation, respectively. The error bar on each bar chart indicates the average RMSE and the 95% CI bounds. It is shown that parameters that result in RMSE above the baseline of 1.151% are considered highly impactful, whereas those below the baseline indicate a weaker influence on the model's decision-making. The feature importance analysis aligned with the directional relationship identified in the Pearson correlation, confirming that capacity and R_{ct} maintained positive correlations, while R_w, R_s, and R_O exhibited negative correlations. In terms of predictive importance, capacity proved to be the most critical feature, yielding an RMSE [1.153 ± 0.0006]. Among the impedance parameters, R_w was the most impactful, yielding an RMSE of [1.152 ± 0.0004]. The R_{ct} parameter sat squarely at the baseline with an RMSE of [1.151±0.0006]. In contrast, R_s they R_O fell below the baseline, recording RMSE values of [1.15±0.0001] and [1.143 ±0.0004], respectively. Ultimately, the LSTM-derived feature importance successfully mirrored the Pearson correlation results, mutually validating R_w as the most significant parameter.

D. Degradation mechanism diagnosis

To interpret these data-driven findings physically, a diagnosis of the degradation mechanism was conducted. This approach maps the relationship between resistance parameters and specific electrochemical degradation pathways, as established in the literature (Fig. 8), providing critical insights into the degradation behavior of Cell 5 during its initial 100 cycles.

Starting with the R_O parameter, it exhibited the weakest negative correlation and the lowest predictive importance in the LSTM model. This suggests that severe macroscopic degradation, such as extensive active material isolation (contact loss) or massive electrolyte dry-out, has not yet predominantly manifested at this early stage of battery cycling, during the first 100 cycles. The R_s parameter demonstrated a slightly higher, yet still moderate impact compared to R_O. This indicates that while standard SEI layer thickening and potentially mild lithium plating were occurring due to the aggressively high C-rate, they are not the primary drivers of capacity fade.

Significantly, $R_w$emerged as the most critical degradation factor, demonstrating both the strongest negative correlation and the highest feature importance. This highlights the severe impact of the 100% DOD and 2.5 C-rate cycling conditions. Such aggressive lithium-ion extraction and insertion could induce structural strain and a drastic phase transition in the active electrode materials. Consequently, solid-state diffusion of lithium ions was strongly hindered, confirming R_w as the primary mechanism behind early capacity loss [2, 8].

Finally, R_{ct} showed an anomalous positive correlation, indicating that charge-transfer resistance decreased with declining SOH. While elevated temperatures can exponentially increase reaction kinetics, heat accumulation was confidently ruled out because the EIS measurements were consistently conducted at a controlled 25°C following a sufficient 30-minute rest period. Therefore, the phenomenon is best explained by cell activation and the deep electrolyte wetting phase. The continuous, extreme volume expansion and contraction – often referred to as electrode breathing - caused by 100% DOD cycling forces the electrolyte to penetrate deeper into the porous electrode structure. This deep penetration could expose fresh micro-cracks and previously inactive sites, temporarily increasing the electrochemically active surface area and resulting in a lowering R_{ct} during the initial 100 cycles [8, 12].

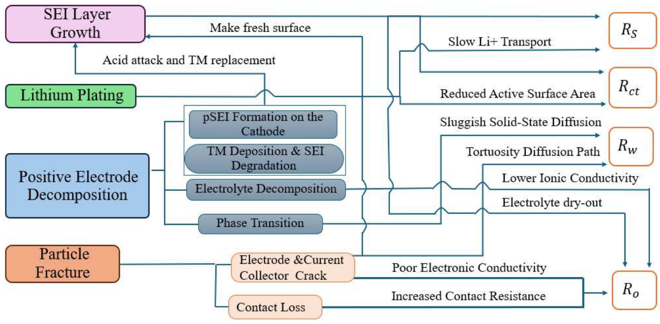

Fig. 8. The degradation mechanism is affected by resistance

CONCLUSION

This study presents a comprehensive diagnostic framework integrating Electrochemical Impedance Spectroscopy (EIS), Pearson correlation, and a Long Short-Term Memory (LSTM) network to evaluate early-stage degradation in commercial NMC lithium-ion batteries under aggressive cycling conditions. By bridging the gap between data-driven models and electrochemical behavior, the results identify Warburg impedance (R_w) as the dominant parameter governing early capacity fade (r = −0.668 ± 0.119), confirming that severe structural strain impedes solid-state lithium diffusion. In contrast, the charge transfer resistance (R_{ct}) exhibits a positive correlation (r = 0.379 ± 0.187), attributed to an activation phase in which electrode volume expansion enhances electrolyte penetration and interfacial kinetics. The minimal predictive contribution of R_o and $R_s$indicates that macroscopic material isolation and severe electrolyte dry-out have not yet developed at this stage.

While this explainable AI framework offers a solid foundation for advanced Battery Management Systems (BMS), implementing real-time EIS- and ECM-based curve fitting in electric vehicles (EVs) entails practical hurdles, including high computational demands and inverter-induced signal noise. These challenges could be addressed by performing scheduling analysis during idle charging times or by using pre-computed lookup tables. Additionally, since validation in this study relies on continuous cycling data with SoH values around 92.5%, the diagnostic reliability may vary in real-world scenarios with intermittent data collection. As degradation mechanisms are expected to change as the battery approaches its automotive End of Life (EOL) threshold (70–80% SoH), future work will expand experimental protocols to track these transitions and assess the framework's robustness up to EOL.

ACKNOWLEDGMENT

This work is financially supported by the Takahashi Industrial and Economic Foundation in Fiscal Year 2024 and by the Special Endowed Course for Green Industrial Transformation towards Sustainability, funded by the AEM-METI Economic & Industrial Cooperation Committee (AMEICC). The authors also appreciate the support from Mr. Amornthep Sing-se for his invaluable assistance in facilitating the experiments.

REFERENCES

[1] Maite Etxandi-Santolaya, Lluc Canals Casals,Cristina Corchero, "Extending the electric vehicle battery first life: Performance beyond the current end of life threshold," *Heliyon,* vol. 10, no. 5, p. Article number e26066, 2024.

[2] J. S. E. e. al, "Lithium ion battery degradation: what you need to know," *Phys. Chem.,* pp. pp. 8200-8221, 2021.

[3] Sarawut Pongha , Boonyarit Seekoaon , Wanwisa Limphirat, Pinit Kidkhunthod , "XANES Investigation of Dynamic Phase Transition in Olivine Cathode for Li-Ion Batteries," *Advanced Energy Materials,* vol. 5, no. 19, p. Article number 1500663, 2015.

[4] O. Haas, A. Deb, E. J. Cairns, A. Wokaun, "X-Ray Absorption Study of $LiFePO_4$ Electrodes," *Journal of The Electrochemical Society,* vol. 152, no. 1, pp. A191-A196, 2005.

[5] N., C. Nayak, Kruti K. Halankar, S.N. Jha, D. Bhattacharyya, "First results of in-situ X-ray Absorption Spectroscopy study on charging-discharging cycles of lithium ion battery at Indus-2 SRS," *Nuclear Instruments and Methods in Physics Research Section A: Accelerators, Spectrometers, Detectors and Associated Equipment,* vol. 972, no. C, p. Article number 164032, 2020.

[6] Gennady Cherkashinin, Kristian Nikolowski, Helmut Ehrenberg,Lucangelo Dimessoa ,Wolfram Jaegermann, "The stability of the SEI layer, surface composition and the oxidation state of transition metals at the electrolyte–cathode interface impacted by the electrochemical cycling: X-ray photoelectron spectroscopy investigation," *Physical Chemistry Chemical Physics,* vol. 14, pp. 12321-12331, 2012.

[7] Yuta Kimura, Aina Tomura, Mahunnop Fakkao, Takashi Nakamura, Nozomu Ishiguro, Oki Sekizawa, Kiyofumi Nitta, Tomoya Uruga, Toyoki Okumura, Mizuki Tada, Yoshiharu Uchimoto, Koji Amezawa, "3D Operando Imaging and Quantification of Inhomogeneous Electrochemical Reactions in Composite Battery Electrodes," *The Journal of Physical Chemistry Letters,* 2020.

[8] Pietro Iurilli , Claudio Brivio, Vanessa Wood, "On the use of electrochemical impedance spectroscopy to characterize and model the aging phenomena of lithium-ion batteries: a critical review," *Journal of Power Sources,* vol. 505, p. Article number 229860, 2021.

[9] Evgenij Barsoukov, J. Ross Macdonald, "Impedance Spectroscopy: Theory, Experiment, and Applications," in *Fundamentals of Impedance Spectroscopy*, Canada, Wiley-Interscience (John Wiley & Sons, Inc., 2005, pp. 80,414.

[10] Alasdair J. Crawford,Daiwon Choi, Patrick J. Balducci,Venkat R. Subramanian,Vilayanur V. Viswanathan, "Lithium-ion battery physics and statistics-based state of health model," *Journal of Power Sources,* vol. 501, 2021.

[11] Aakanksha, A. Sahoo, A. K. Sharma, and Y. Sharma,, "Physics based modeling of LiFePO4 cathodes: effects of electrode parameters on cell performance during fast charging," *J. Phys. Energy,* vol. vol. 5, p. Art. no. 045013, , 2023.

[12] Woosung Choi, Heon-Cheol Shin, Ji Man Kim, Jae-Young Choi, Won-Sub Yoon, "Modeling and Applications of Electrochemical Impedance Spectroscopy (EIS) for Lithium-ion Batteries," *Journal of Electrochemical Science and Technology,* vol. 11, no. 1, pp. 1-13, 2020.

[13] J. Li, K. Adewuyi, N. Lotfi, R.G. Landers, J. Park, "A single particle model with chemical/mechanical degradation physics for lithium ion battery State of Health (SOH) estimation," *Applied Energy,* vol. 212, p. 1178–1190, 2018.

[14] Phattara Khumprom , Nita Yodo, "A Data-Driven Predictive Prognostic Model for Lithium-ion Batteries based on a Deep Learning Algorithm," *Phattara Khumprom (corresponding author), Nita Yodo,* vol. 12, no. 4, 2019.

[15] Juncheng Fu, Zhengxiang Song , Jinhao Meng , Chunling Wu, "Prediction of Lithium-Ion Battery State of Health Using a Deep Hybrid Kernel Extreme Learning Machine Optimized by the Improved Black-Winged Kite Algorithm," *Batteries,* vol. 10, no. 11, 2024.

[16] Kun Li, Xinling Chen, "Machine Learning-Based Lithium Battery State of Health Prediction Research," *Applied Sciences,* vol. 14, no. 2, 2024.

[17] Jiang, Y.H., Yu, Y.F., Huang, J.Q., Cai, W.W., Marco, J.,, " Li-ion battery temperature estimation based on recurrent neural networks," *Science China Technological Sciences,* p. 64, 2021.

[18] Jingdong Lin, Guansong Yan, Chang Wang, "Li-ion battery state of health Prediction based on Long Short-Term Memory Recurrent Neural Network," *Journal of Physics: Conference Series,* vol. 2020, no. 1, p. 012133, 2021.

[19] Kyungnam Park, Yohwan Choi, Won Jae Choi, Hee-Yeon Ryu, Hongseok Kim, "LSTM-Based Battery Remaining Useful Life Prediction With Multi-Channel Charging Profiles," *IEEE Access,* vol. 8, pp. 20786-20798, 2020.

[20] "Electrochemical Impedance Spectroscopy: A New Chapter in the Fast and Accurate Estimation of the State of Health for Lithium-Ion Batteries," *Ming Zhang,Yanshuo Liu,Dezhi Li,Xiaoli Cui, Licheng Wang, Liwei Li, and Kai Wang,* vol. 16, no. 4, p. 1599, 2023.

[21] "Identifying degradation patterns of lithium ion batteries from impedance spectroscopy using machine learning," *Yunwei Zhang, Qiaochu Tang, Yao Zhang, Jiabin Wang, Ulrich Stimming, Alpha A. Lee,* vol. 11, p. 1706, 2020.

[22] Jichang Peng, Ya Gao, Lei Cai, Ming Zhang, Chenghao Sun, Haitao Liu, "State of Health Estimation for Lithium-Ion Batteries Using Electrochemical Impedance Spectroscopy and a Multi-Scale Kernel Extreme Learning Machine," *World Electric Vehicle Journal,* vol. 16, no. 4, p. 224, 2025.